Morphological characterization of bicontinuous structures in polymer blends and microemulsions by the inverse-clipping method in the context of the clipped-random-wave model

Hiroshi Jinnai,[1,*] Yukihiro Nishikawa,[1,†] Sow-Hsin Chen,[2] Satoshi Koizumi,[3] and Takeji Hashimoto[1]
[1]*Hashimoto Polymer Phasing Project, ERATO, Japan Science and Technology Corporation, Kyoto 606-8501, Japan and Department of Polymer Chemistry, Graduate School of Engineering, Kyoto University, Kyoto 606-8501, Japan*
[2]*Department of Nuclear Engineering, Massachusetts Institute of Technology, 24-209, Cambridge, Massachusetts 02139*
[3]*Advanced Science Research Center, Japan Atomic Energy Research Institute, Tokai-mura, Ibaraki 319-1195, Japan*
(Received 20 October 1999)

A method is proposed to determine the spectral function of the clipped-random-wave (CRW) model directly from scattering data. The spectral function $f(k)$ (k is a wave number) gives the distribution of the magnitude of wave vectors of the sinusoidal waves that describes the essential features of the two-phase morphology. The proposed method involves ''inverse clipping'' of a correlation function to obtain $f(k)$ and does not require any *a priori* assumptions for $f(k)$. A critical test of the applicability of the inverse-clipping method was carried out by using three-component bicontinuous microemulsions. The method was then used to determine $f(k)$ of the bicontinuous structure of a phase-separating polymer blend. $f(k)$ for the polymer blend turned out to be a multipeaked function, while $f(k)$ for the microemulsions exhibits a single broad maximum representing periodicity of the morphology. These results indicate the presence of the long-range regularity in the morphology of the polymer blend. Three-dimensional (3D) morphology corresponding to the scattering data of the polymer blend was generated using the CRW model together with the multipeaked $f(k)$. Interface curvatures of the 3D morphology calculated from $f(k)$ were measured and compared with those experimentally determined directly from the laser scanning confocal microscopy in the same blend.

PACS number(s): 68.35.Ct, 42.30.Wb, 47.20.Hw, 83.70.Hq

I. INTRODUCTION

Studies of bicontinuous structures in nature have been an attractive research theme. They are formed in a variety of condensed-matter systems, such as binary mixtures of polymers, simple liquids, metallic alloys, and inorganic glasses in the course of phase separation called spinodal decomposition (SD) [1,2]. In other cases, bicontinuous equilibrium structures are formed in microemulsions (where the structures are spatially disordered) [3,4], lyotoropic cubic phases of amphiphilic systems [5], and microphase-separated block copolymers [6] (both spatially ordered).

The bicontinuous structures of polymer blends have been extensively studied by measuring characteristic lengths, e.g., the characteristic wavelength of concentration fluctuations, Λ_m. Since one of the dominant driving forces of the phase separation is the reduction of an excess interfacial free energy associated with the interface area, studies of local shape and its time evolution are required. Hence interface related quantities, such as interface area per unit volume and interface thickness, were determined by scattering techniques [7,8]. Until recently, however, one of the most essential interface related parameters, i.e., interfacial curvatures, was not able to be determined. We quantitatively measured the interface curvatures on the basis of the differential geometry from the three-dimensional (3D) image of the interface obtained by using laser scanning confocal microscopy (LSCM) [9]. Unfortunately, however, it is sometimes difficult to experimentally obtain 3D interface structures due to some experimental difficulties; for example, some structures may be too small (nanometer scale rather than micrometer scale), or some samples may be too turbid to observe under (optical) microscopy. Even though the size of the structure is below the resolution of the optical microscopy, it may still be possible to obtain 3D structural images by employing transmission electron microscopy (TEM) combined with computer tomography. This technique, however, requires extensive and complicated sample preparation.

It would be convenient if one could estimate 3D interfacial structures directly from scattering data. In the scattering experiments, it is feasible to ''tune'' the wave number (and thus the observable spatial scale) by changing the wavelength of the incident radiation, which may reduce the experimental difficulty associated with the microscopy mentioned above. Note that the magnitude of the wave number is defined as

$$q \equiv (4\pi/\lambda)\sin(\theta/2), \tag{1}$$

where λ and θ are, respectively, the wavelength of the incident beam and scattering angle in the medium.

A ''clipped-random-wave (CRW)'' model was first proposed by Cahn in order to generate 3D structures formed via SD [10]. The model was later modified by Berk to analyze scattering data and generate 3D structures corresponding to the scattering data [11]. A random Gaussian field generated by superposing many sinusoidal waves with random phases and with their wave vectors oriented in all directions with

*Present address: Department of Polymer Science and Engineering, Kyoto Institute of Technology, Matsugasaki, Kyoto 606-8585, Japan. Electronic address: hjinnai@ipc.kit.ac.jp
†Present address: Structural Biophysics Laboratory, The Institute of Physical and Chemical Research (RIKEN), 1-1-1 Kouto, Mikaduki, Sayo, Hyogo 679-5148, Japan.

equal probabilities is ''clipped'' to generate the two-phase morphology. In the framework of the CRW model, an essential feature of the structure is incorporated through a function called spectral function in Fourier space, which describes the distribution of the sinusoidal waves with the magnitude of the wave vectors, k. The function may differ from system to system.

The CRW model has been used extensively to analyze the scattering data in three-component (water/oil/surfactant) microemulsions. Chen *et al.* [4] proposed a peaked spectral function [described later in Eq. (7)], which was able to quantitatively reproduce their small-angle neutron scattering (SANS) profiles of the microemulsions. Furthermore, the CRW model, along with Chen's spectral function (hereafter referred to as a modified-Berk, or MB model) was used to estimate the area-averaged Gaussian curvature, $\langle K \rangle$, of the microemulsions [12].

The MB model was also applied to a polymer blend. The model reasonably reproduced a light-scattering (LS) profile of the blend in the late stage SD [13]. There was a resemblance between the structure of the polymer blend and that of the microemulsions, despite the fact that these two systems differ in the characteristic length scale by a factor of about 250. We note here that the length scale of the polymer blend is typically of the order of micrometers, whereas that of the microemulsions is of the order of 100 Å. In the q region smaller than the q at scattering maximum, q_m, the scaled intensity of the polymer blend was weaker than that of the MB model at the corresponding q region. The scattering intensity profile at the low-q region may be related to the thermal noise of the system. The more the thermal noise plays a substantial role, the stronger the scattering intensity becomes. Hence the thermal noise may play a more substantial role in the microemulsions than in the polymer blend. However, until now, a fundamental question as to whether or not Chen's spectral function, used to analyze the LS data of the polymer blend is an appropriate function, has remained unsolved.

In the present paper, we propose a method to estimate the spectral function *directly* from the scattering data without any assumptions. The spectral function derived from the scattering data of a polymer blend will be compared with that of microemulsions in order to discuss fundamental differences between the two systems. In addition, a 3D interface generated from the spectral function in the context of the CRW model will be presented (Sec. IV D). Interface curvatures calculated from the generated 3D interface will be compared with the results obtained from the corresponding *real* 3D interface taken by the laser scanning confocal microscopy.

II. THEORETICAL BACKGROUND

In general, the intensity distribution of LS and SANS from an isotropic two-component (e.g., A and B) porous material can be calculated from a Debye correlation function, $\Gamma(r)$, by the following formula:

$$I(q) = \langle \eta^2 \rangle \int_0^\infty 4\pi r^2 \Gamma(r) \frac{\sin(qr)}{qr} dr, \tag{2}$$

where $\langle \eta^2 \rangle = v_A v_B (\rho_A - \rho_B)^2$. v_A and v_B refer to the volume fractions of the phases rich in A and B. ρ_A and ρ_B denote, respectively, the corresponding refractive indices for LS and the scattering lengths for SANS. There are two physical boundary conditions: $\Gamma(r \to 0) = 1$ and $\Gamma(r \to \infty) = 0$. Besides these conditions, the most important property of $\Gamma(r)$ is that it has a linear term in the small r expansion to ensure a finite interfacial area per unit volume, S/V:

$$\Gamma(r \to 0) = 1 - \frac{1}{4 v_A v_B} \frac{S}{V} r + \cdots. \tag{3}$$

Cahn proposed a scheme for generating a 3D morphology of a phase-separated A-B alloy by clipping a Gaussian random field generated by superposing many isotropically directed sinusoidal waves with random phases [10]. Later, Berk further extended Cahn's idea for the purpose of analyzing scattering data [11]. An important relation between the two-point correlation function in the random Gaussian field and the Debye correlation function was derived. In Berk's original paper, however, he only discussed a spectral function that is a δ function [11]. This produced a morphology that is only partially disordered.

In the random wave model of Berk, the Gaussian random field $\psi(\vec{r})$ is constructed by the following sum:

$$\psi(\vec{r}) = \frac{1}{\sqrt{N}} \sum_{i=1}^{N} \cos(\vec{k}_i \cdot \vec{r} + \varphi_i), \tag{4}$$

where the directions of the wave vector $\vec{k}_i$ are sampled isotropically over a unit sphere and the phase φ_i is distributed randomly over the interval $(0, 2\pi)$. Note that the Gaussian random field is normalized so that the field describing the local concentration of A and B fluctuates continuously between -1 and 1 as $N \to \infty$. The statistical properties of the Gaussian random process are completely characterized by giving its two-point correlation function $g(|\vec{r}_1 - \vec{r}_2|) = \langle \psi(\vec{r}_1) \psi(\vec{r}_2) \rangle$. The associated spectral function $f(k)$ is related to it by the Fourier transformation

$$g(|\vec{r}_1 - \vec{r}_2|) = \int_0^\infty 4\pi k^2 f(k) \frac{\sin(k|\vec{r}_1 - \vec{r}_2|)}{k|\vec{r}_1 - \vec{r}_2|} dk. \tag{5}$$

Note $f(k)$ describes the essential features of the morphology.

This $\psi(\vec{r})$ function representing a continuous Gaussian random field is then clipped to generate an interface and thus results in the two-phase morphology. The correlation function $\Gamma(r)$, representing a two-state-discrete random field, is then obtained from $g(r)$ via the van Vleck transformation given by Eq. (6) below. Namely, the field assigns -1 to all negative signals representing A and $+1$ to all positive signals representing B. Then $\Gamma(r)$ for this discrete random field (i.e., an ideal random two-phase system) for the isometric case, namely $v_A = v_B$, is given as

$$\Gamma(r) = \frac{2}{\pi} \sin^{-1}[g(r)]. \tag{6}$$

In this way, $\Gamma(r)$ has a linear term in the small r expansion.

A suitable form of the spectral function for the microemulsions was proposed by Chen *et al.* [4], which is an inverse sixth-order polynomial in k containing three parameters: a, b, and c. It is

$$f_{\mu E}(k)=\frac{8\pi b[a^2+(b+c)^2]/(2\pi)^3}{(k^2+c^2)[k^4-2(a^2-b^2)k^2+(a^2+b^2)^2]}. \quad (7)$$

This form is an extension of the well-known structure factor proposed by Teubner and Strey for bicontinuous microemulsions [14]. The corresponding two-point correlation function can be written down analytically using Eq. (5) and has a quadratic term in the small r expansion:

$$g(r)=\frac{1}{a^2+(c^2-b^2)}\left\{(a^2+c^2-b^2)\frac{\sin(ar)}{ar}e^{-br}+2b\frac{e^{-cr}-e^{-br}\cos(ar)}{r}\right\}$$
$$=1-\frac{1}{6}\left\{\frac{(a^2+b^2)^2+c^2(a-b)(a+3b)}{a^2+(c-b)^2}\right\}r^2+\cdots. \quad (8)$$

$\Gamma(r)$ can be calculated from this $g(r)$ using Eq. (6). The intensity distribution of LS and SANS can be calculated by $\Gamma(r)$ using Eq. (2). The parameters a, b, and c are evaluated by fitting the scattering intensity distribution to the experimentally observed scattering data. The first two parameters, a and b, have their approximate correspondence in the Teubner-Strey theory (''TS theory''). In the TS theory, the Debye correlation function is given by $\Gamma_{TS}(r)=e^{-r/\xi}[\sin(2\pi r/d)/(2\pi r/d)]$. The correspondences are $a\approx 2\pi/d$ and $b\approx 1/\xi$, where d is the interdomain repeat distance and ξ the coherence length of the local order. The parameter c controls the transition to the large q behavior of the scattering intensity, which may be related to the persistence length of the interface.

As mentioned in Sec. I, although the spectral function $f_{\mu E}(k)$ for the microemulsions [Eq. (7)] reproduced the LS function of a polymer blend to some extent, it remains unclear whether or not $f_{\mu E}(k)$ is an appropriate one. One way to avoid this problem is to find the spectral function from the scattering data *without any assumption*. Equations (2) and (5) are the spherical Fourier transformation and the reversible operation, respectively. Hence $\Gamma(r)$ can be found by using the inverse Fourier transformation; i.e.,

$$\Gamma(r)=\int_0^\infty 4\pi q^2 I(q)[\sin(qr)/qr]dq/\langle\eta^2\rangle. \quad (9)$$

$g(r)$ can then be obtained using the following relation because the ''clipping'' operation of Eq. (6) is mathematically reversible:

$$g(r)=\sin[(\pi/2)\Gamma(r)]. \quad (10)$$

We refer to this operation as the ''inverse-clipping'' method. The spectral function $f(k)$ is now evaluated by the inverse operation of Eq. (5):

$$f(k)=\int_0^\infty 4\pi k^2 g(r)[\sin(kr)/kr]dr. \quad (11)$$

Thus the spectral function can be found directly from the experimental scattering profiles without any *a priori* assumption.

III. EXPERIMENTS

The polymer blend used in the present study was a mixture of perdeuterated polybutadiene (DPB) and polybutadiene (PB) at the critical composition. Both polymers were synthesized by living anionic polymerization. The number-average molecular weight (M_n) of DPB was 128×10^3. The heterogeneity index for a molecular weight distribution, M_w/M_n (M_w is the weight-averaged molecular weight), was 1.12. PB had $M_n=88.9\times10^3$ and $M_w/M_n=1.07$. The DPB/PB mixtures with a composition of 46 wt. % DPB and 54 vol % PB were dissolved in benzene and lyophilized. Note that the DPB/PB blend has an upper critical solution temperature-type phase diagram whose critical temperature is approximately 110 °C. The mixture was annealed at 40 °C for 1675 min. The phase-separated structure was observed in 3D by using laser scanning confocal microscopy (Carl Zeiss, LSM410^{TM}) [15]. The optical axis of the microscopy, which is perpendicular to the focal plane (x-y plane), is defined as the z axis. Experimental details can be found elsewhere [16].

Ternary mixutures of heavy water (D_2O), *n*-octane, and tetraethylene glycol monodecyl ether (C_4E_{10}) were used. Volume fractions of the surfactant (ϕ_s), water (ϕ_w), and oil (ϕ_o) were, respectively, 0.132, 0.434, and 0.434. For a nonionic surfactant of this type, a variety of structures are formed due to the balance between the hydrophilicity and the hydrophobicity in the ternary system. There is a range of temperatures where the hydrophobic nature of the hydrocarbon tail of the surfactant is nearly matched by the hydrophilicity of the molecular head group. At such temperatures, the one-phase microemulsion becomes thermodynamically stable. For the particular concentration of surfactant used here, the one-phase region [17] spans the temperature range from about 18.3 to 21.3 °C. The microstructure consists of interpenetrating domains of water and oil, having characteristic dimensions of the order of 10 nm, with most of the surfactant molecules sitting at the interface.

SANS measurements were carried out for the microemulsion at the JRR-3M Research Reactor, Japan Atomic Energy Research Institute (JAERI), Tokai-mura, using the SANS-J instrument. A monochromatic neutron beam of wavelength $\lambda=0.435$ nm was used. The samples were mounted on a temperature controlled four-position sample changer under the control of the instrument computer. Neutrons scattered by the microemulsions were recorded on a two-dimensional area detector, software coded as 128×128 pixels. Two different detector positions from the sample were used, i.e., 1.35 m and 6 m, in order to expand the q range. The definition of q is given by Eq. (1).

IV. RESULTS AND DISCUSSION

A. Test of validity of the ''inverse-clipping'' method

Let us first compare $f(k)$, calculated directly from the inverse-clipping method described in Sec. II, and $f_{\mu E}(k)$,

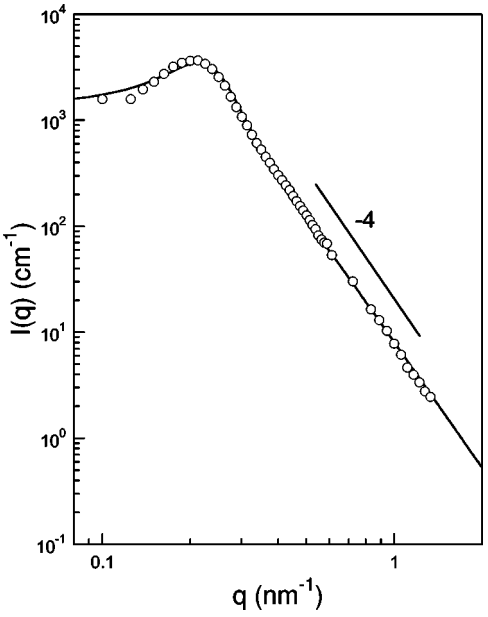

FIG. 1. SANS profile $I(q)$ (○) of the microemulsion (H_2O/n-octane/E_4C_{10}). The solid line is a best fit of modified-Berk model ($a=2.28\times10^{-1}$ nm^{-1}, $b=6.93\times10^{-2}$ nm^{-1}, $c=5.82\times10^{-1}$ nm^{-1}).

obtained based on the MB model for the microemulsion system. Figure 1 shows SANS intensity distribution $I(q)$ as a function of q for the microemulsion at 20.3 °C. The open circles and the solid line in the figure represent the SANS profile and the best fit of the MB model to the data, respectively. $f_{\mu E}(k)$ was used in the fitting. As shown in Fig. 1, the MB model quantitatively reproduced the experimentally obtained SANS intensity distribution. The obtained parameters were $a=2.28\times10^{-1}$ nm^{-1}, $b=6.93\times10^{-2}$ nm^{-1}, $c=5.82\times10^{-1}$ nm^{-1}. We now define a quantity (called a disorder parameter), b/a, which is $(1/2\pi)(d/\xi)$. This parameter shows the relative ratio between the periodicity of the order and the coherence length of the local order. The disorder parameter for the microemulsion shown in Fig. 1 turned out to be 0.3, which is in agreement with the previous value obtained from the same microemulsion at a similar composition and temperature; i.e., $b/a=0.25$ [13].

As proposed in Sec. II, $f(k)$ was calculated from the inverse-clipping method. In the actual calculation, the SANS intensity $I(q)$ was first extrapolated in such a way that the asymptotic scattering behavior shows q^n and q^{-4} in the q regions smaller and larger than the q value at the scattering maximum q_m, respectively, as shown by the solid line in Fig. 2(a), in which n was set to zero in this particular case. The extrapolation was necessary for the accurate estimation of $\Gamma(r)$ through the inverse Fourier transformation of $I(q)$ [Eq. (9)], the inverse clipping of $\Gamma(r)$ [Eq. (10)], and the inverse Fourier transformation of $g(r)$ [Eq. (11)].

In Fig. 2(b), $f(k)$ thus evaluated directly from $I(q)$ is presented as the solid line. Note that $f(k)$ did not rely on any kinds of assumptions. The dotted line in Fig. 2(b) shows $f_{\mu E}(k)$ *independently* calculated by inserting the three length parameters obtained from the fitting (see the solid line in Fig. 1) of the MB model to Eq. (7). $f_{\mu E}(k)$ thus obtained showed a single broad peak with the asymptotic behavior of q^{-6} in the high-q region. The spectral functions evaluated from the two independent methods *quantitatively* agreed over the wide intensity range as large as three orders of magnitude, which shows the validity of the application of the inverse-clipping method to obtain $f(k)$.

B. Fitting the structure factor by the MB model in the phase-separated DPB/PB mixtures

In our previous study [13], $f_{\mu E}(k)$ was used to fit a LS profile from a bicontinuous phase-separated structure of a mixture of polyisoprene (PI) and DPB. It was found that the MB model was able to capture the essential morphological features of the bicontinuous structure. In the present paper, we will use the structure factor of the DPB/PB mixture having the critical composition in the late stage of SD (annealed at 40 °C for 1675 min), which was obtained in the following way: The 3D phase-separated structure of the DPB/PB mixture was observed by LSCM (presented later in Fig. 6). In the LSCM measurements, the interface between the DPB rich and PB-rich phases was obtained in 3D. The structure factor $S(q)$ of the DPB/PB mixture was obtained by using the 3D Fourier transformation [18]. $S(q)$ of the DPB/PB mixture is shown to be in quantitative agreement with the structure factor obtained from a computer simulation based on the time-dependent Ginzburg-Landau equation with hydrodynamic effects [19]. Therefore the DPB/PB blend is one of the best experimental systems to represent a model of

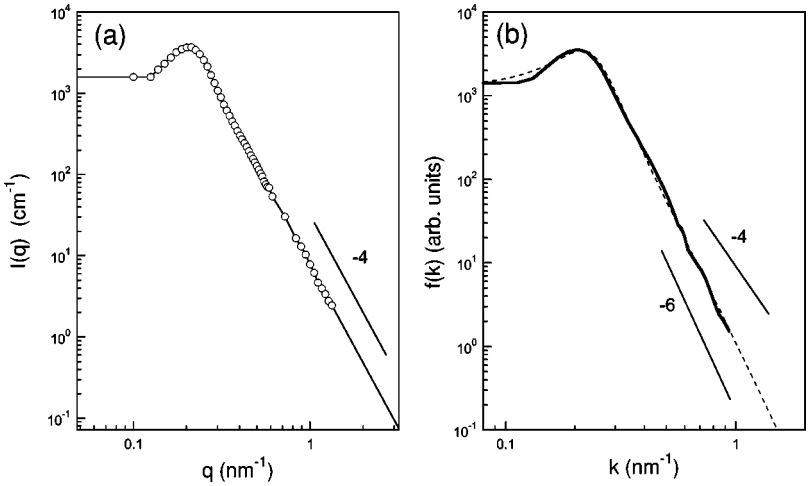

FIG. 2. (a) SANS profile $I(q)$ (○) and extrapolated profile for the inverse-clipping method (solid line) of the microemulsions. The extrapolation was performed as $I(q)=$ const in small q and $I(q)\propto q^{-4}$ in large q. (b) Spectral functions $f(k)$ obtained from the inverse-clipping method (solid line) and modified-Berk fitting (dotted line: $a=5.55\times10^{-1}$ μm^{-1}, $b=1.64\times10^{-1}$ μm^{-1}, $c=1.10$ μm^{-1}).

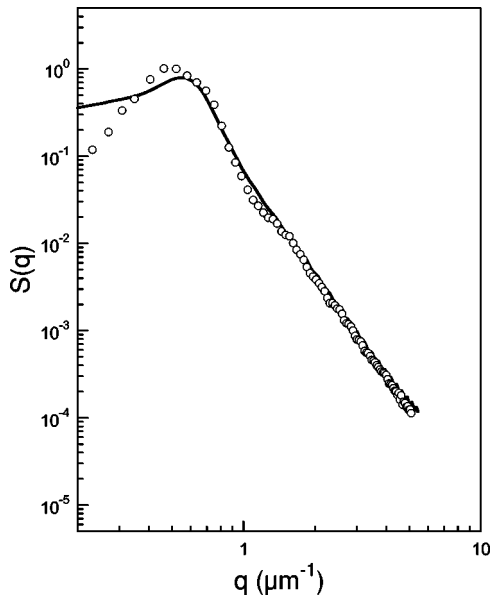

FIG. 3. Structure factor $S(q)$ of the phase-separated DPB/PB blend (○). The solid line is a best fit of modified-Berk model.

binary fluid mixtures, and thus $S(q)$, used here, has universal features in common with them [20].

Let us first demonstrate the fitting of $S(q)$ by the MB model, i.e., the CRW model with $f_{\mu E}(k)$ [Eq. (7)]. In Fig. 3, the open circles and the solid line show, respectively, $S(q)$ obtained from the LSCM experiment and the best fit by the MB model. The MB model reasonably described $S(q)$ of the bicontinuous structure (see Fig. 3), especially in the q region satisfying $q>q_m$. The MB model, however, failed to reproduce the scattering profile in the q region smaller than q_m: The structure factor of the polymer mixture showed q^4 behavior [see also Fig. 4(a) and related comments later], while the MB model predicted q^0. Moreover, the weak scattering maximum or ''shoulder'' appeared in $S(q)$ of the DPB/PB blend at around $q\simeq 1.8\ \mu\mathrm{m}^{-1}\sim 3q_m$, which was less apparent in the MB model. Note that these features were also observed in the fitting of the MB model to the DPB/PI blend [13]. Three parameters, $a=5.55\times10^{-1}\ \mu\mathrm{m}^{-1}$, $b=1.64\times10^{-1}\ \mu\mathrm{m}^{-1}$, and $c=1.10\ \mu\mathrm{m}^{-1}$, were obtained from the fit. The disorder parameter b/a was approximately 0.3, which is somewhat larger than the value obtained from the DPB/PI blend; i.e., $b/a=0.16$ [13].

Although the MB model captures overall features of the structure factor of the DPB/PB mixture as described in the preceding paragraph, the fit was not perfect. Considering the fact that the microemulsion is an equilibrium structure while the phase-separated structure of the DPB/PB mixture is a transient one, and thus the physical origin of the formation of the structures is different, the spectral function originally proposed for the microemulsion, i.e., $f_{\mu E}(k)$, may not be appropriate to describe the morphological features of the polymer mixture. As for the symmetric or nearly symmetric polymer mixtures, the time-dependent Ginzburg-Landau model [19] gives a better prediction than the MB model.

C. Spectral function of the DPB/PB phase-separated polymer mixture

We now apply the inverse-clipping method to the structure factor obtained from the phase-separated DPB/PB mixture. Figure 4(a) shows $S(q)$ used for the evaluation of the spectral function, $f_{blend}(k)$, intrinsic to the bicontinuous structure of the DPB/PB polymer blend by the inverse-clipping method. The open circles represent $S(q)$, obtained from the 3D LSCM structure with the Fourier transformation. It was extrapolated in such a way that $S(q)$ had q^4 and q^{-4} in the q region smaller and larger than q_m, respectively. q^{-4} is the Porod scattering representing the existence of the sharp interface [21–23]. q^4 is a prediction from the theories of Yeung [24] and Furukawa [25] for spinodally decomposed bicontinuous structures for the conserved-order parameter system.

The spectral function $f_{blend}(k)$ determined directly from $S(q)$ of the DPB/PB mixture is presented in Fig. 4(b) (solid line). For comparison, the spectral function for the DPB/PB blend evaluated from the MB model, which was calculated from $f_{\mu E}(k)$, together with the three parameters obtained from the fitting presented in Fig. 3, are displayed as a dotted line. The two spectral functions show a qualitative agreement. An agreement was obtained in the asymptotic behavior of k^{-6} at $k>k_m$. Here k_m is the wave number at which $f(k)$ becomes a maximum. However, we note the following two important differences between them. One of the most significant differences between the two spectral functions is that $f_{blend}(k)$ showed a distinct second-order maximum at k

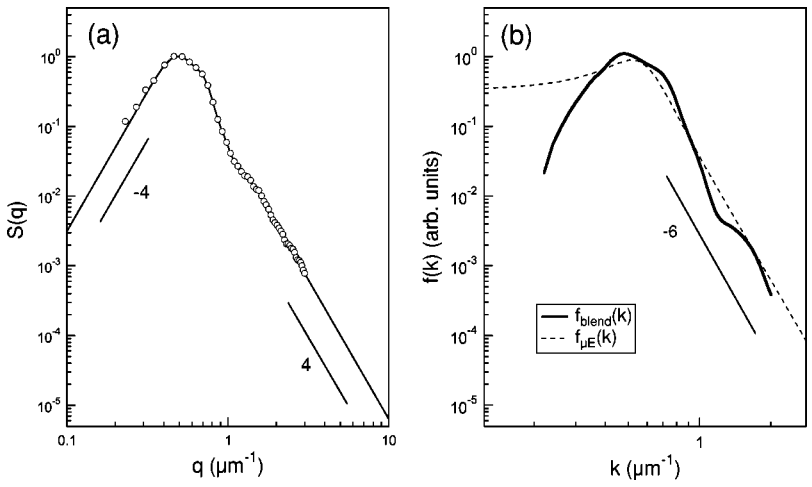

FIG. 4. (a) Structure factor (○) and extrapolated profile for the polymer blend (solid line). The extrapolation was performed as $I(q)\propto q^4$ in small q and $I(q)\propto q^{-4}$ in large q. (b) Spectral functions obtained from the inverse-clipping method, $f_{blend}(k)$ (solid line), and modified-Berk fitting, $f_{\mu E}(k)$ (dotted line).

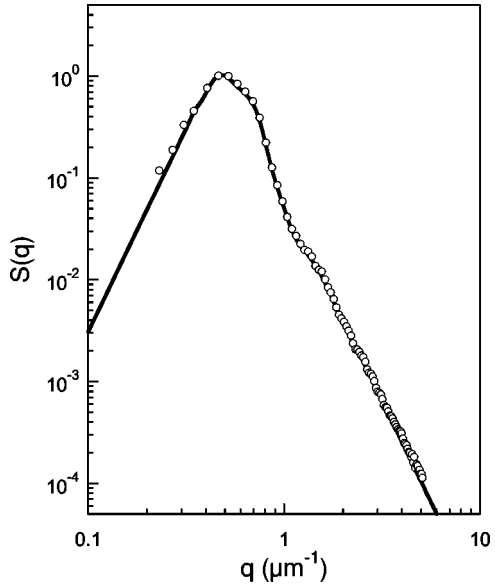

FIG. 5. Comparison of the structure factor $S(q)$ (○) and that calculated from the CRW model with the spectral function estimated by the inverse-clipping method, $f_{blend}(k)$ (solid line).

$\sim 3k_m$. It is intriguing that the second-order maximum was indistinctly observed in $S(q)$ (see Fig. 3) at about the same position, while it is even more emphasized in $f_{blend}(k)$. This result indicates that the regularity in the periodic structure is higher in the DPB/PB mixture than that in microemulsions. Besides the above difference, we note a difference in the asymptotic behavior of $f_{\mu E}(k)$ at $k<k_m$: $f_{blend}(k)\sim k^6$ and $f_{\mu E}(k)\sim k^0$. The structure factor calculated using $f_{blend}(k)$ is demonstrated in Fig. 5. As expected, $S(q)$ (open circles) is quantitatively described in the framework of the CRW model (solid line), if the spectral function is appropriate.

We note in the microemulsion that the spectral function obtained from the inverse-clipping method agrees quite well with $f_{\mu E}(k)$, obtained from the MB fitting as demonstrated in Fig. 2(b). On the other hand, the two spectral functions for the phase-separated structure in the polymer mixture show larger discrepancies, as shown in Fig. 4(b). The fundamental difference between the two systems may be found in the applicability of the spectral function earlier in Eq. (7): The Chen model is less applicable to the polymer mixture than to the microemulsion, though the CRW model works quite satisfactorily for both systems with an appropriate choice of spectral functions.

D. 3D morphology of the DPB/PB blend generated by the CRW model and interface curvature measurements

The 3D interface *experimentally* observed by the LSCM is presented in Fig. 6(a). The box size is 76.8 μm $\times$76.8 μm$\times$38.4 μm in the *X*, *Y*, and *Z* directions, respectively. The interface between the DPB- and PB-rich phases is drawn in 3D; the interface colored by gray faces toward the PB-rich phase, while the one colored by white faces toward the DPB-rich phase. The interdomain repeat distance *d* estimated from the relation $d\approx 2\pi/q_m$ was 11.5 μm.

The CRW model is good for creating 3D structures that are consistent with the measured scattering data as long as the system is isometric and the area-averaged mean curvature

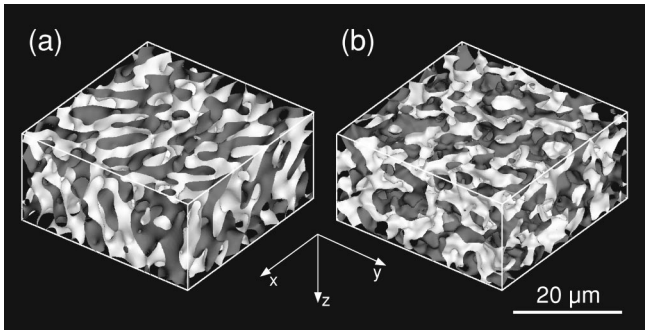

FIG. 6. (a) 3D reconstructed image of the DPB/PB blend by LSCM. (b) 3D generated image using the CRW model based on the spectral function obtained form the inverse-clipping method, $f_{blend}(k)$, that was originally estimated from the LSCM 3D structure. The volume is 76.8 μm$\times$76.8 μm$\times$38.4 μm for each image.

is zero [26]. Figure 6(b) demonstrates the 3D morphology for the DPB/PB polymer blend obtained from $f_{blend}(k)$ on the basis of the CRW model. We used Eq. (4) with $N\sim 2\times 10^4$. The repeat distance of the bicontinuous structure was around 11.3 μm, which was obtained from the relation $d\approx 2\pi/k_m$. The interface observed from the LSCM experiments (''LSCM interface'') appeared to be smoother than that generated by the CRW model (''CRW interface''). We emphasize here that the structure factor obtained from the 3D CRW interface quantitatively agreed with that of the LSCM interface.

In order to quantify the interface geometry of the 3D morphology generated by the CRW model, probability densities of the interface curvatures were measured. Details of the method can be found elsewhere [16,27]. Two kinds of curvatures, i.e., the mean, *H*, and the Gaussian, *K*, curvatures, are defined at a point on the interface. They are

$$H=\frac{\kappa_1+\kappa_2}{2},\quad K=\kappa_1\kappa_2. \tag{12}$$

Here κ_1 and κ_2 represent the two principal curvatures at a point of interest on the interface where the curvatures are measured. The local geometry around the point is characterized by the signs and magnitudes of the curvatures. For example, a spherical interface, a typical example of the elliptic surface, has positive *K* and the sign of *H* indicates whether the spherical domain is a DPB-rich phase or vice versa. The parabolic interface, e.g., a lamellar interface, has zero Gaussian curvatures. A hyperbolic interface, such as a saddlelike surface, has a negative *K*. It was found that the roughness of the interface affects the accuracy of the curvature measurements [28]. An index RI, indicating the relative roughness of the interface to the averaged curvature, was introduced as a measure of the roughness of the interface (see Table I) [28]. In generating the CRW interface, the size of the voxel was varied so that the interface had an RI similar to the LSCM interface. Many points on the interface ($\sim 10^5$) were randomly selected in the curvature measurements, from which the joint probability density $P(H,K)$ was determined. $\int\int P(H,K)dHdK=1$ was used for normalization. The shape of the joint probability density was invariant with further

TABLE I. Summary of interface related quantities.

	CRW model	LSCM
ϕ	0.5[a]	0.48 ± 0.01
$S/V\,(\mu\mathrm{m}^{-1})$	0.258	0.231 ± 0.006
RI [b]	0.067	0.065
$\langle H\rangle\,(\mu\mathrm{m}^{-1})$	0.009 ± 0.008	0.012 ± 0.009
$\sigma_H\ (\mu\mathrm{m}^{-1})$	0.233 ± 0.010	0.145 ± 0.018
$\langle K\rangle\,(\mu\mathrm{m}^{-2})$	-0.0575 ± 0.0045	-0.0799 ± 0.0103
$\sigma_K\,(\mu\mathrm{m}^{-2})$	0.154 ± 0.007	0.140 ± 0.018
$d\,(\mu\mathrm{m})$	11.3	11.5 ± 1.5

[a]Assumption in the CRW model.

[b]RI is defined as $\sqrt{\langle A_\Delta\rangle}(|\langle\kappa_1\rangle|+|\langle\kappa_2\rangle|)/2$, where $\langle A_\Delta\rangle$ is the average area of the triagles constituting the interface. RI is an index to measure the roughness of the interface [28].

sampling. From $P(H,K)$, the probability densities of the mean curvature, $P_H(H)$, and that of the Gaussian curvature, $P_K(K)$, were also calculated:

$$P_H(H)\equiv\int P(H,K)dK,\quad P_K(K)\equiv\int P(H,K)dH. \tag{13}$$

Figure 7 shows $P_H(H)$ (a) and $P_K(K)$ (b) for the 3D interface experimentally measured by LSCM (shown by triangles) and that generated from the CRW model for the DPB/PB mixture during the SD (shown by circles). Since $f_{blend}(k)$ was used to generate the CRW interface, the probability densities of curvatures are expected to be same between the two 3D interfaces. Overall features of the probability densities are similar: (i) $P_H(H)$ is symmetrical about $H=0$. The area-averaged mean curvature $\langle H\rangle$ was essentially zero for both interfaces. (ii) $P_K(K)$ distributed mostly in the $K<0$ region, demonstrating that the interface is hyperbolic. The area-averaged Gaussian curvature $\langle K\rangle$ showed good agreement for both interfaces. $\langle H\rangle$ and $\langle K\rangle$ are listed in Table I.

However, there exist quantitative discrepancies between the two 3D interfaces. $P_H(H)$ for the CRW interface is considerably broader than that for the LSCM interface. The standard deviation of H, σ_H, for the CRW interface, was larger than that for the LSCM interface by a factor of 1.6 (see Table I). The standard deviation of the Gaussian curvature, σ_K, was a little bit larger for the CRW interface. One of the major differences is the fact that the portion of $K>0$, i.e., the elliptic surface, in $P_K(K)$ for the CRW interface ($\sim$26.8%) was considerably larger than that for the LSCM interface ($\sim$7.2%). These results indicate that the CRW interface has an excess asperity of the interface, equally concave and convex to one of the phase-separated domains, compared with the LSCM interface.

Let us now compare the area-averaged curvatures obtained from three independent methods: We obtained $\langle K\rangle$ to be -0.0575 and $-0.0799\ \mu\mathrm{m}^{-2}$ from the LSCM, the inverse-clipping method, respectively. Following a theorem proposed by Teubner [29], i.e., $\langle K\rangle=-(1/6)\langle k^2\rangle$, $\langle K\rangle=-0.0855\,\mu\mathrm{m}^{-2}$ was obtained for the DPB/PB mixture. Namely, the second moment of the spectral function is related to the Gaussian curvature. In Teubner's method,

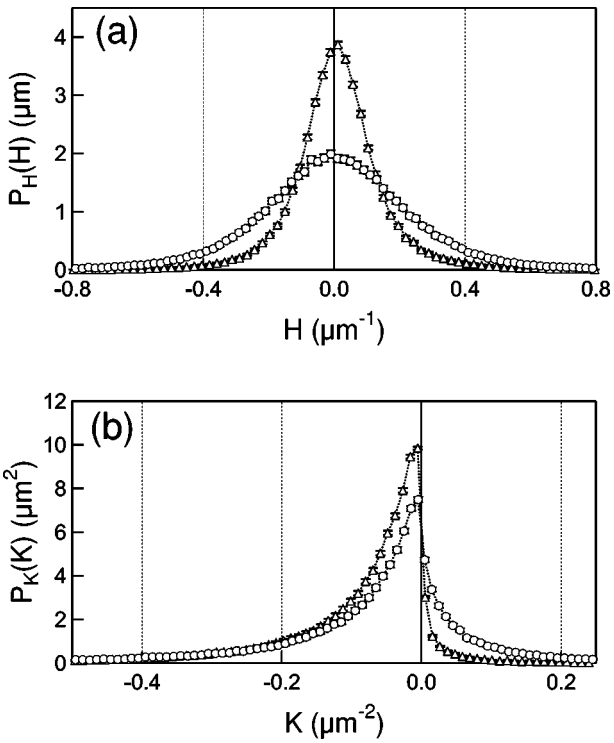

FIG. 7. Probability densities of (a) mean curvature $P_H(H)$ and (b) Gaussian curvature $P_K(K)$ obtained from the CRW model together with $f_{blend}(k)$ (○) and those from LSCM 3D interface (△).

$f_{\mu E}(k)$ and the three parameters obtained in the fitting shown in Fig. 3, were used to estimate the $\langle K\rangle$. The essential difference between the two area-averaged Gaussian curvatures from the inverse-clipping method and Teubner's method is the difference between the spectral functions used in the estimation. The principal curvatures roughly estimated from $\langle K\rangle$ via $\sqrt{-\langle K\rangle}$ are, respectively, 0.239, 0.282, and 0.292 $\mu\mathrm{m}^{-1}$ for the LSCM , the inverse-clipping method, and Teubner's method. Thus, as far as the area-averaged curvatures are concerned, both the inverse-clipping method and the MB model gave about 20% error compared with the true value obtained from the LSCM. Note that $\langle H\rangle$ is essentially zero for every method.

V. CONCLUSIONS

Within the framework of the clipped-random-wave model, a method (''inverse-clipping method'') was proposed to determine the spectral function $f(k)$ from scattering data without any *a priori* assumptions. The spectral function describes the essential features of two-phase morphologies and thus has central importance in the CRW model. Small-angle neutron scattering data from a three-component microemulsion was used to test the validity of the method. The spectral function obtained from the inverse-clipping method came out in excellent agreement with the one proposed by Chen *et al.* [4], which has so far been used extensively to explain the scattering data in microemulsions.

The inverse-clipping method was then applied to estimate the spectral function of the bicontinuous structures of a polymer blend. A three-dimensional (3D) image of the interface was obtained by laser scanning confocal microscopy. The

structure factor was calculated by taking a 3D Fourier transformation of the 3D LSCM image of the interface, from which the spectral function $f_{blend}(k)$ was obtained by the inverse-clipping method. It had a shoulderlike maximum at $k \sim 3k_m$, demonstrating a high regularity of the periodicity of the structure. This is in strong contrast with the spectral function for the microemulsions that has only a single broad maximum. This result demonstates that the thermal noise plays a more significant role in microemulsions than in the polymer blend.

A 3D image of the interface was generated with the knowledge of $f_{blend}(k)$, which was subjected to the curvature distribution measurements. The obtained curvature distributions were compared with those experimentally evaluated from the LSCM 3D image. Overall features of the morphology were successfully reproduced by the CRW model with $f_{blend}(k)$. However, it seems that the CRW model generated excess asperity to the interface; the standard deviation of the mean curvature was considerably larger for the CRW interface than for the LSCM interface, and a large portion of the interface belonged to the elliptic surface. As far as the area-averaged values are concerned, the area-averaged mean radius of the interface differs by about 20%, which is reasonable under some assumptions made in the CRW model.

A method of finding out the real-space morphology of an interfacial structure in porous materials is appealing in general to researchers in complex fluids. For systems with micrometer length scales, LSCM can be used to obtain the interfacial structures *experimentally*. However, for 100-Å scale structures, one needs to use SANS and somehow find a way to visualize the possible morphology that is consistent with the scattering data. The CRW model is one of the answers to the problem. It is the theory for any arbitrary isotopic porous material, if we know how to find the spectral function. So far, one class of spectral function applicable to this special class of materials, e.g., microemulsions, is known. The inverse-clipping method proposed in the present paper offers the way to find the spectral function *directly* from the scattering data without any assumption (except for isotopic structures). Comparisons between 3D structures observed by experimental methods such as LSCM and the CRW model with the inverse-clipping method deserve further study to test the availability of the CRW model not only for the nonequilibrium systems, e.g., polymer blends, but also for equilibrium systems.

ACKNOWLEDGMENTS

This work was performed under the JAERI Collaboration Research Program. This work was partially supported by the Ministry of Education, Science, Sports and Culture, Japan (Grant-in-Aid No. 11305067).

[1] J. D. Gunton, M. S. Miguel, and P. S. Sahni, in *Phase Transition and Critical Phenomena*, edited by C. Domb and J. L. Lebowitz (Academic Press, New York, 1983), p. 269.
[2] T. Hashimoto, Phase Transit. **12**, 47 (1988).
[3] W. Jahn and R. Strey, J. Phys. Chem. **92**, 2294 (1988).
[4] S. H. Chen, D. D. Lee, and S. L. Chang, J. Mol. Struct. **296**, 259 (1993).
[5] S. T. Hyde, Curr. Opin. Solid State Mater. Sci. **1**, 653 (1996).
[6] H. Hasegawa, H. Tanake, K. Yamasaki, and T. Hashimoto, Macromolecules **20**, 1651 (1987); H. Jinnai, Y. Nishikawa, R. J. Spontak, S. D. Smith, D. A. Agard, and T. Hashimoto, Phys. Rev. Lett. **84**, 518 (2000).
[7] T. Hashimoto, T. Takenaka, and H. Jinnai, J. Appl. Crystallogr. **24**, 457 (1991).
[8] M. Takenaka and T. Hashimoto, J. Chem. Phys. **96**, 6177 (1992).
[9] H. Jinnai, T. Koga, Y. Nishikawa, T. Hashimoto, and S. T. Hyde, Phys. Rev. Lett. **78**, 2248 (1997).
[10] J. W. Cahn, J. Chem. Phys. **42**, 93 (1965).
[11] N. F. Berk, Phys. Rev. Lett. **58**, 2718 (1987).
[12] S. H. Chen, D. D. Lee, K. Kimishima, H. Jinnai, and T. Hashimoto, Phys. Rev. E **54**, 6526 (1996).
[13] H. Jinnai, T. Hashimoto, D. Lee, and S. H. Chen, Macromolecules **30**, 130 (1997).
[14] M. Teubner and R. Strey, J. Chem. Phys. **87**, 3195 (1987).
[15] T. Wilson, in *Confocal Microscopy*, edited by T. Wilson (Academic Press, London, 1990).
[16] H. Jinnai, Y. Nishikawa, H. Morimoto, T. Koga, and T. Hashimoto, Langmuir (to be published).
[17] Note here that the term ''one-phase'' microemulsion does not necessarily imply that the three components are miscible at the molecular level. It only means that the system is not macroscopically phase separated. In the one-phase microemulsion, at moderate surfactant concentration, it is known that a microphase-separated structure exists in *thermal equilibrium*.
[18] The structure factor was calculated from $S(q) \sim |F(q)|^2$ and $F(q) \sim \mathcal{F}(c(r))$, where $F(q)$ and $c(r)$ are the structure amplitude and spatial distribution of the local concentration fluctuations (e.g., PB=1 and DPB=0) in 3D. $\mathcal{F}(c(r))$ shows the Fourier transformation of $c(r)$. Note that $S(q)$ is proportional to the scattering intensity, $I(q)$.
[19] T. Koga and K. Kawasaki, Physica A **196**, 389 (1993).
[20] T. Hashimoto, H. Jinnai, Y. Nishikawa, T. Koga, and M. Takenaka, Prog. Colloid Polym. Sci. **106**, 118 (1997).
[21] G. Porod, Kolloid-Z. **124**, 83 (1951).
[22] G. Porod, Kolloid-Z. **125**, 51 (1952).
[23] G. Porod, Kolloid-Z. **125**, 108 (1952).
[24] C. Yeung, Phys. Rev. Lett. **61**, 1135 (1988).
[25] H. Furukawa, Phys. Rev. B **40**, 2341 (1989).
[26] D. D. Lee and S. H. Chen, Nuovo Cimento D **16**, 1357 (1994).
[27] Y. Nishikawa, T. Koga, H. Jinnai, and T. Hashimoto (unpublished).
[28] Y. Nishikawa, H. Jinnai, T. Koga, T. Hashimoto, and S. T. Hyde, Langmuir **14**, 1242 (1998).
[29] M. Teubner, Europhys. Lett. **14**, 403 (1991).